Iraqi Journal of Physics, 2022 *Vol. 20, No. 1, PP. 26-36*
DOI: 10.30723/ijp.v20i1.961 *P-ISSN:2070-4003*
E-ISSN:2664-5548

Preparation of a Composite of Copper Oxide Nanoparticles with Carbon by Exploding Graphite Rod in Aqueous Suspension

Sawsan H. Abdulla[1a], Hammad R. Humud[2b], Falah I. Mustafa[3c]
[1,2]Department of Physics, College of Science, University of Baghdad, Baghdad, Iraq
[3]Ministry of Science and Technology, Baghdad, Iraq
[b]E-mail: dr.hammad6000@yahoo.com, [c]E-mail: mustafafalah@gmail.com
[a*]Corresponding author: sawsanhussein1976@gmail.com

Abstract

In this work, the effect of preparing a composite of copper oxide nanoparticles with carbon on some of its optical properties was studied. The composite preparing process was carried out by exploding graphite electrodes in an aqueous suspension of copper oxide. The properties of the plasma which is formed during the explosion were studied using emission spectroscopy in order to determine the most important elements that are present in the media. The electron's density and their energy, which is the main factor in the composite process, were determined. The particle properties were studied before and after the exploding process. The XRD showed an additional peak in the copper oxides pattern corresponding to the hexagonal graphite structure for the composite. The UV-visible absorbance for the composite was significantly enhanced. The direct bandgap decreased from 2.55 to 2.4 eV, and the indirect bandgap decreased from 1.1 to 1 eV, for the composite.

Article Info.

Keywords:
CuO: C particles, Graphite, exploding, Plasma characteristics, Stark broadening.

Article history:
Received: Nov. 09, 2021
Accepted: Jan. 31, 2022
Published: Mar. 01,2022

1. Introduction

Plasma emission spectrometry is a simple and well-known method to characterize plasma properties. The plasma emission spectrum displays spectral lines corresponding to electronic transitions between atomic or ionic energy levels [1]. The intensity of the spectral lines depends on many parameters namely electron temperature (T_e), probability of transition (A_{ji}) between the corresponding levels $j \rightarrow i$, and statistical weight of the excited state level (g_j), as shown by the Boltzmann distribution [2]:

$$\boldsymbol{I_{ji} = \frac{N}{U(T)} g_j A_{ji} h\nu_{ji} e^{-E_j/k_B T_e}} \quad \textbf{(1)}$$

where E_j and E_i represents the upper and lower energy levels, respectively and k_B is the Boltzmann constant.

So, the electron temperature can be calculated using Boltzmann plot [3]:

$$\boldsymbol{Ln\left(\frac{I_{ji}\lambda_{ji}}{g_j A_{ji}}\right) = \left(-\frac{E_j}{KT_e}\right) + \left(\frac{N(T)}{U(T)}\right)} \quad \textbf{(2)}$$

where λ_{ji} is the wavelength emitted by the transition from j to i level. The electron density in plasma is calculated, using the line broadening by Stark effect [4]:

$$\boldsymbol{n_e(cm^{-3}) = \left[\frac{\Delta\lambda}{2\omega_s(\lambda, T_e)}\right] N_r} \quad \textbf{(3)}$$

where $\Delta\lambda$ represents the full width of a spectral line, and ω_s is the electron effect parameter, Nr is the reference electron density equal to 10^{16} (cm^{-3}) for atoms and 10^{17} (cm^{-3}) for ions.

The distance beyond which the electric field of a charged particle within plasma is shielded is known as the Debye length λ_D:

$$\boldsymbol{\lambda_D = \sqrt{\frac{\varepsilon_0 k_B T_e}{n_e e^2}}} \quad \textbf{(4)}$$

where ε_0 is the permittivity of free space and e is the electron charge. The collective behaviour condition is realized when $L >> \lambda_D$, where L signifies the geometrical size of the plasma. In addition, the number of electrons within the Debye sphere must be greater than unity:

$$\boldsymbol{N_D = \frac{4\pi n_e}{3}\lambda_D^3 \gg 1} \quad \textbf{(5)}$$

The third condition for the collective response depends on electron oscillation frequency, or as called plasma frequency. This parameter plays an essential role in many plasma interactions. The electrons may complete many plasma oscillations before it collides with other heavy plasma species.

$$\boldsymbol{\omega_p = \sqrt{\frac{n_e e^2}{m_e \varepsilon_0}}} \quad \textbf{(6)}$$

where m_e is the electron mass [5].

The exploding wire method is a simple way to generate plasma by passing a high current through a thin wire. Nanoparticles are created by this way when the evaporated material by the exploding process is cooled into the surrounded medium [6]. The exploding wire technique is employed in many studies and applications. One of this, is in the field of nanoparticles generation [7]. It is an effective and simple way to produce economical quantities of nanoparticles of high-purity and of various specifications depending on the preparing conditions. The created particle size can be controlled by changing the applied current, the wire diameter, and the surrounding medium [8].

Kang et al.(2016) [9] synthesized C-encapsulated Ni, Co, and Fe magnetic nanoparticles of onion-like layers by solution plasma processing without any additional treatment. Gaoa et al. (2017) [10] produced Graphene nanosheets by electrical explosion of graphite sticks in distilled water. Characterizations by various techniques show different forms of carbon phases, including graphite nanosheets and mono-layer graphene with good crystallinity.

In this study, the structural and optical properties of the composite which consist from copper oxide and carbon nanoparticles was studied with different copper oxide to carbon nanoparticles ratio.

2. Experimental work

Copper oxide nanoparticles of purity 99.5% (US Research Nanomaterials, Inc.), graphite rod of 0.9 mm diameter and graphite plate were used in this work. Aqueous dispersion was prepared by mixing 0.1 g of the CuO powder with 100 ml distilled water. Exploding wire system of graphite pin-plate configuration was used for C-CuO composite preparing by passing about 100 A DC current through graphite rod when attached with graphite plate inside the aqueous suspension, as shown in the schematic diagram shown in Fig.1.

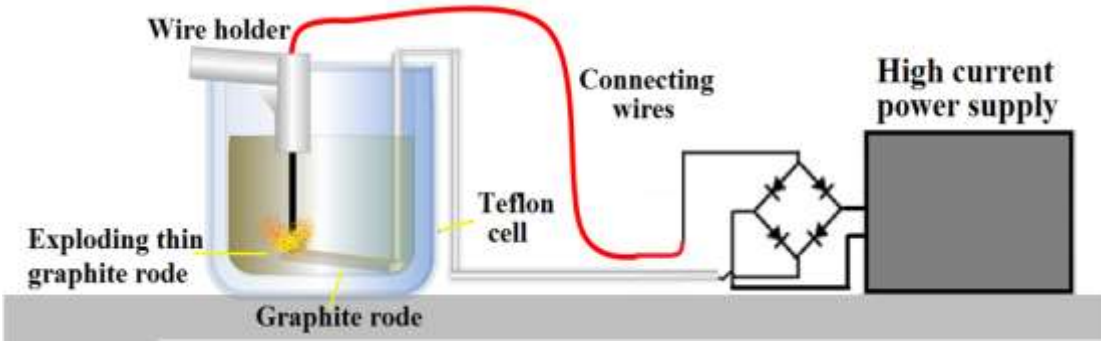

Figure 1: Schematic diagram of the system for exploding carbon rod in aqueous suspension.

Plasma characteristics were studied using the light emitted from the exploding process using optical emission spectroscopy. The emission was transferred by an optical fibre to a spectrometer connected with a computer to be stored and analysed. Glass was used as substrates for drying the prepared C-CuO NPs for more characterization. The prepared C-CuO NPs were examined by the XRD system (Shimadzu XRD 6000), with Cu-Kα source of 1.5405 Å wavelength, using 40 kV voltage and 30.0 mA current. The scanning angle was in the range of (2θ =20-80̊) with a speed of 5 degrees/min. UV-visible spectrometer (Avantes DH-D-BAL-2048 UV-Vis), in the range of 200 to 1100 nm wavelength was used.

3. Results and discussions

3.1. Characterization of C- CuO composite

Fig.2 shows the X-ray diffraction pattern for the graphite rod used in the exploding wire system. The pattern matched the graphite structure (Hexagonal phase) identical with standard card No. 96-900-0047. The preferred peak appeared along the (002) direction at about 26.5° with full width at half maximum of 0.209° as shown in the inset figure.

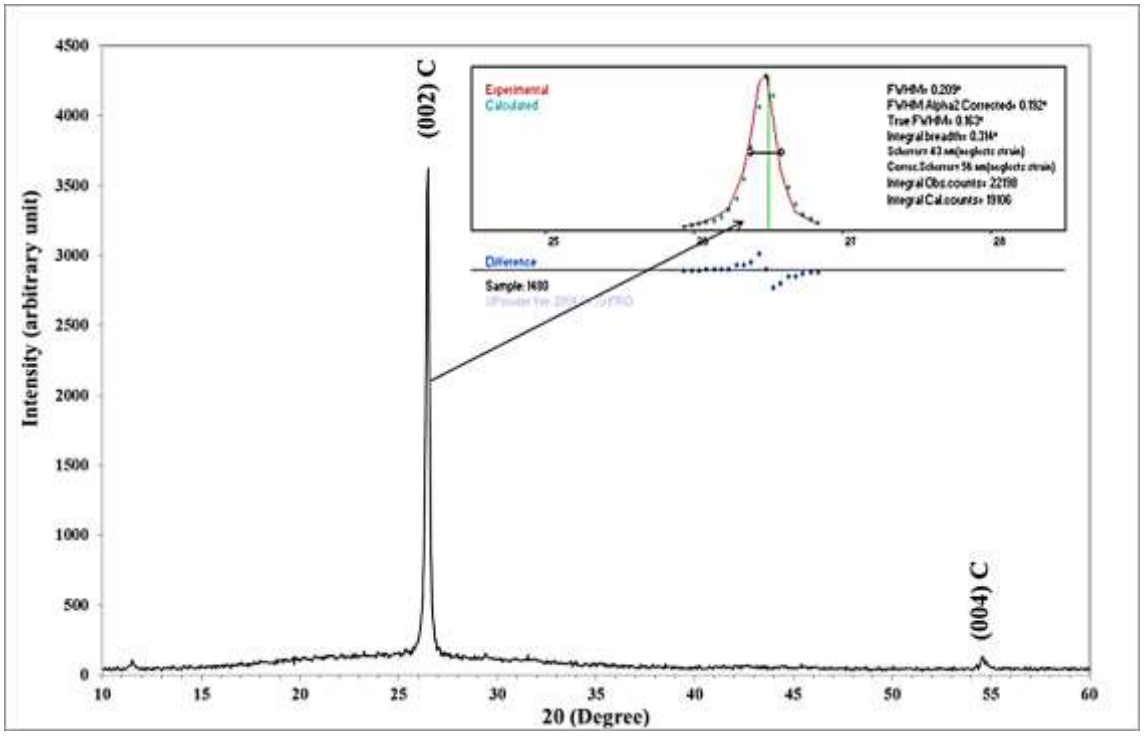

Figure 2: X-ray diffraction pattern of graphite electrode.

Fig.3 shows the X-ray diffraction pattern for C-CuO composite nanoparticles using exploding wire method, deposited on glass substrate by drop-casting and dried at room temperature. The poly-crystalline structure appeared identical with cubic – copper oxide crystals (standard card No. 96-101-1195) with peaks located at 32.1849°, 35.3726°, 38.5603°, 48.5097°, 58.4913°, 61.3891°, 66.1868°, and 75.0092° matched with (110), (11-1), (111), (20-2), (202), (-113), (31-1), and (22-2) lattice planes, respectively. An additional peak appeared at a diffraction angle of 26.4213° corresponding to the (002) plane of hexagonal graphite structure identical with (standard card No. 96-900-0047). The intermolecular planer distances (d_{hkl}) were calculated using Bragg's formula [11] while, the crystallite size (*C.S*) was calculated using Scherrer formula [12].

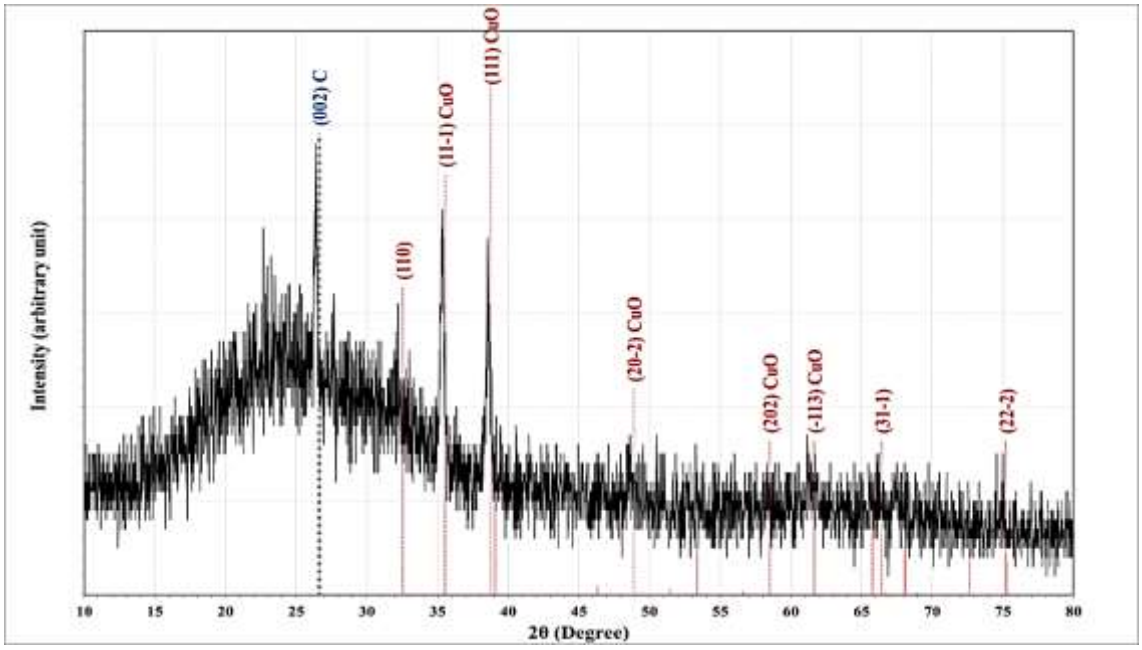

Figure 3: XRD pattern for C-CuO NPs.

Table 1 shows Bragg angles (2θ), full width at half maximum (FWHM), Miller indices (*hkl*), comparison between experimental and standard intermolecular plane distances d_{hkl} values, and crystalline size (*C.S*) for the observed peaks of C-CuO nanoparticles.

Table 1: XRD parameters for CuO nanoparticles compose with carbon using exploding wire method.

2θ (Deg.)	FWHM (Deg.)	d_{hkl} Exp. (Å)	C.S (nm)	d_{hkl} Std.(Å)	hkl	Phase
26.4213	0.3010	3.3706	27.1	3.3447	(002)	Hex.C
32.1849	0.3864	2.7790	21.4	2.7509	(110)	Mono.CuO
35.3726	0.3542	2.5355	23.6	2.5228	(11-1)	Mono.CuO
38.5603	0.4185	2.3329	20.1	2.3212	(111)	Mono.CuO
48.5097	0.2898	1.8751	30.1	1.8617	(20-2)	Mono.CuO
58.4913	0.4830	1.5767	18.9	1.5764	(202)	Mono.CuO
61.3891	0.5473	1.5090	16.9	1.5034	(-113)	Mono.CuO
66.1868	0.4507	1.4108	21.0	1.4061	(31-1)	Mono.CuO
75.0092	0.4186	1.2652	23.9	1.2614	(22-2)	Mono.CuO

Fig. 4 shows the scanning electron microscope images for CuO nanoparticles before and after composite preparation by exploding carbon rod and dried on glass substrate.

The nanoparticles appear irregular in shape and size. The particles of diameters that varied from 1500 to 2500 nm (as measured using Image J software) represents the CuO particles. After the exploding process, the CuO particles appeared attached to small particles of diameter ranging from 300 to 500 nm. Fig.5 shows the EDX analysis, with inset tables showing the elements content of the two samples. It shows the characteristic peaks of the electronic transition of the copper and oxygen, while the composite sample has an additional peak of 44.69 % of carbon. The peak appeared at 1.7 keV corresponding to Si of the glass substrate. There was small variation in O to Cu ratio between the two samples.

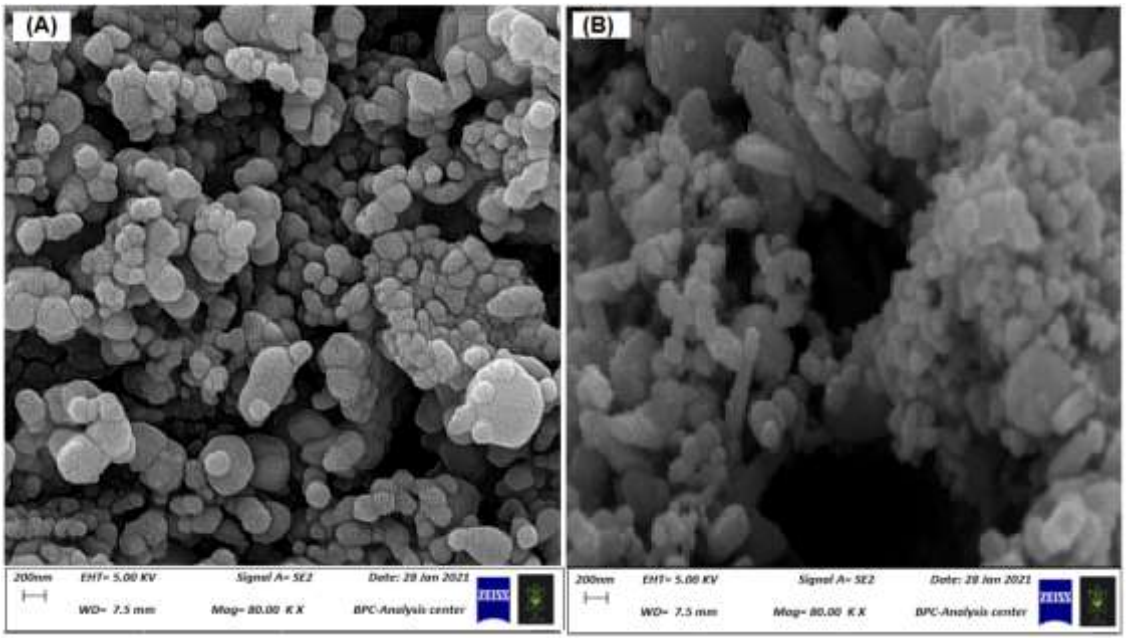

Figure 4: FE-SEM analysis for (A) CuO and (B) C- CuO NPs.

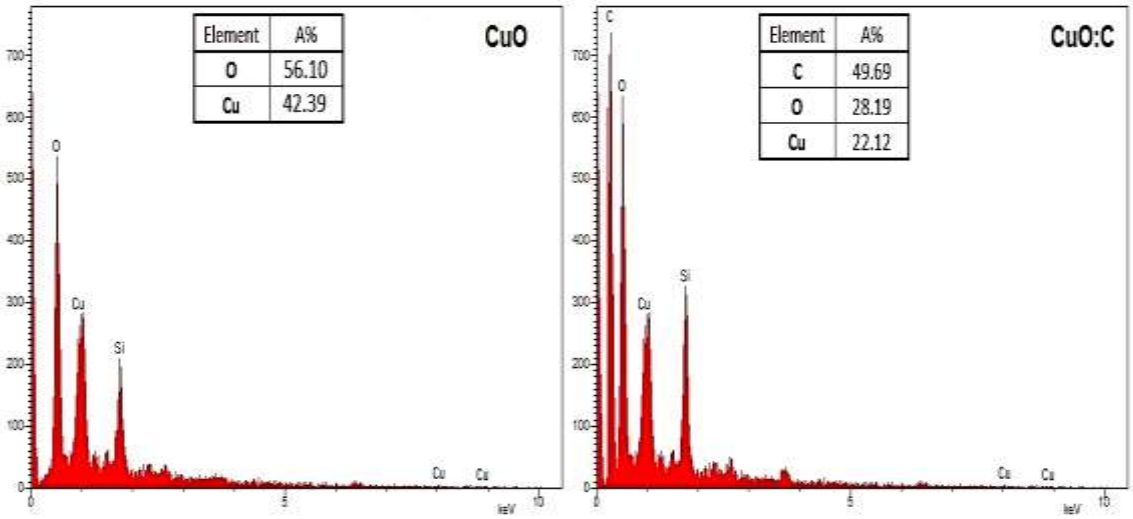

Figure 5: EDX analysis for CuO and C- CuO NPs.

The optical properties of the pure and composite nanoparticles were studied to find out its effect on the optical characteristics. Fig.6 shows the absorbance coefficient patterns, for CuO and C-CuO nanoparticles dried on glass substrates by drop casting, within the wavelength range of (200 –1100) nm. It seems that absorbance has increased with carbon composite. The composite samples could absorb more visible light energy due to the presence of new energy levels within the band gap, as shown in previous studies

[13]. The absorption of CuO NPs improved significantly due to the effect of carbon contents. This agrees with the results of Ding et al. [14] and chen et al. [15].

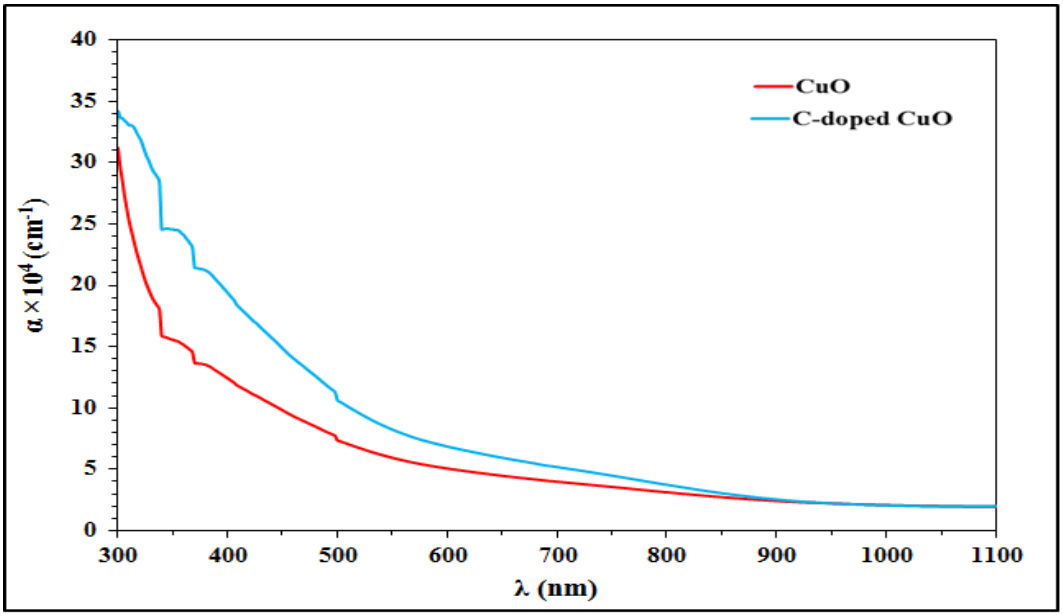

Figure 6: Absorbance efficient curves for CuO and CuO:C nanoparticles dried on glass substrates.

The optical band gaps of copper oxide can either be direct or indirect, depending on their oxidising degree [16]. Fig.7 illustrates the use of *Tauc* relation to calculate the optical band gap (E_g^{opt}) in both manners, direct and indirect. The optical band gap (E_g^{opt}) was determined by extrapolating the linear part of the curve to the x-axis. The direct band gap decreased from 2.55 to 2.4 eV, while, the indirect bandgap decreased from 1.1 to 1 eV after C-CuO composite preparation.

3.2. Plasma Characterization

Fig.8 illustrates the spectroscopic patterns of the emission from exploding thin graphite rods in aqueous suspension of copper oxide powders compared with the standard lines of atomic and ionic emissions for copper, oxygen and, hydrogen (Cu I, C II, OI, and H) [17].

The ionic lines for carbon and the atomic lines for the metal oxide indicates a high degree of ionization by the huge energy delivered to the carbon atoms, while, only part of this energy was transferred to the copper atoms. The H_α line appeared at 653 nm for hydrogen atoms produced from the dissociation of water molecules due to high local energy delivered to the wire at a short time. The different in line intensities is due to the variation of transmission probability and the statistical weight for different levels.

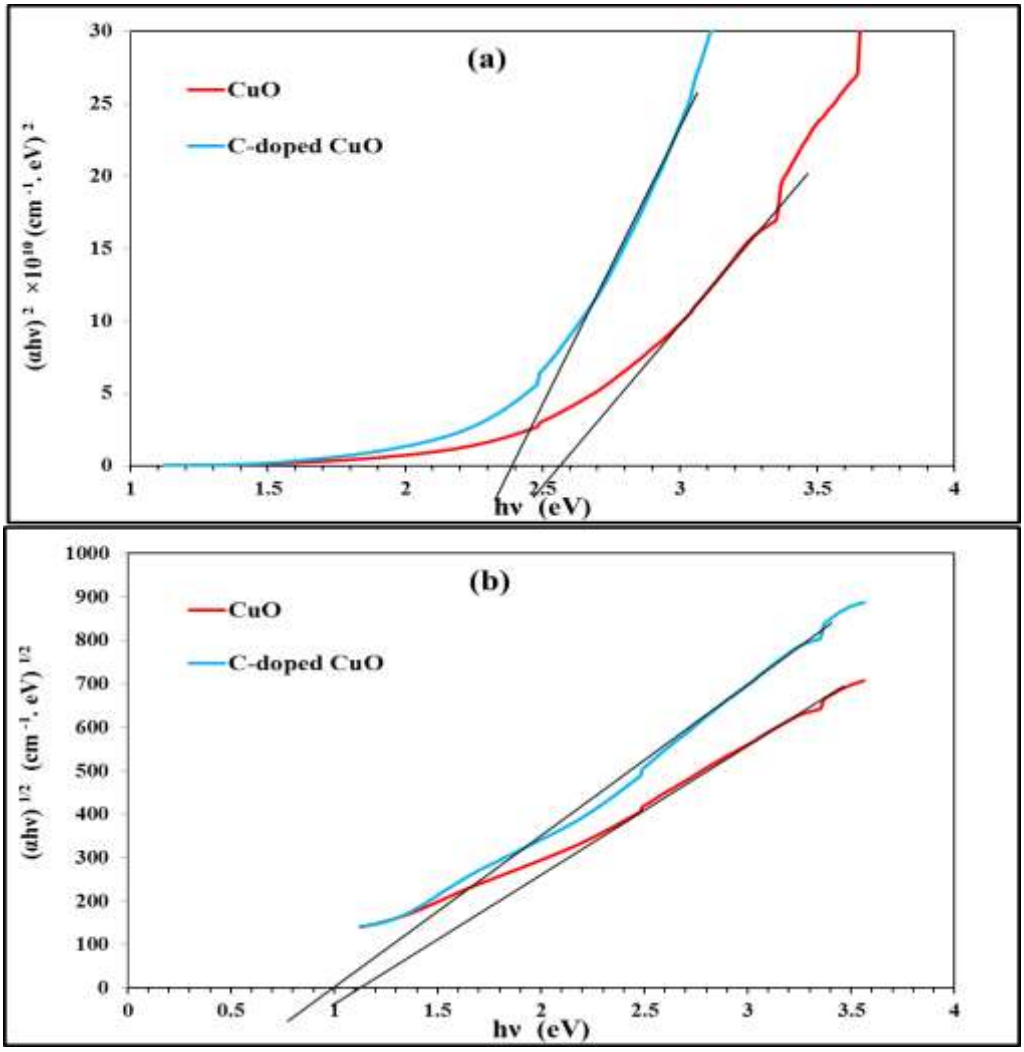

Figure 7: Bandgaps calculation using Tauc relation for (a) direct and (b) indirect transitions for CuO and C-CuO NPs.

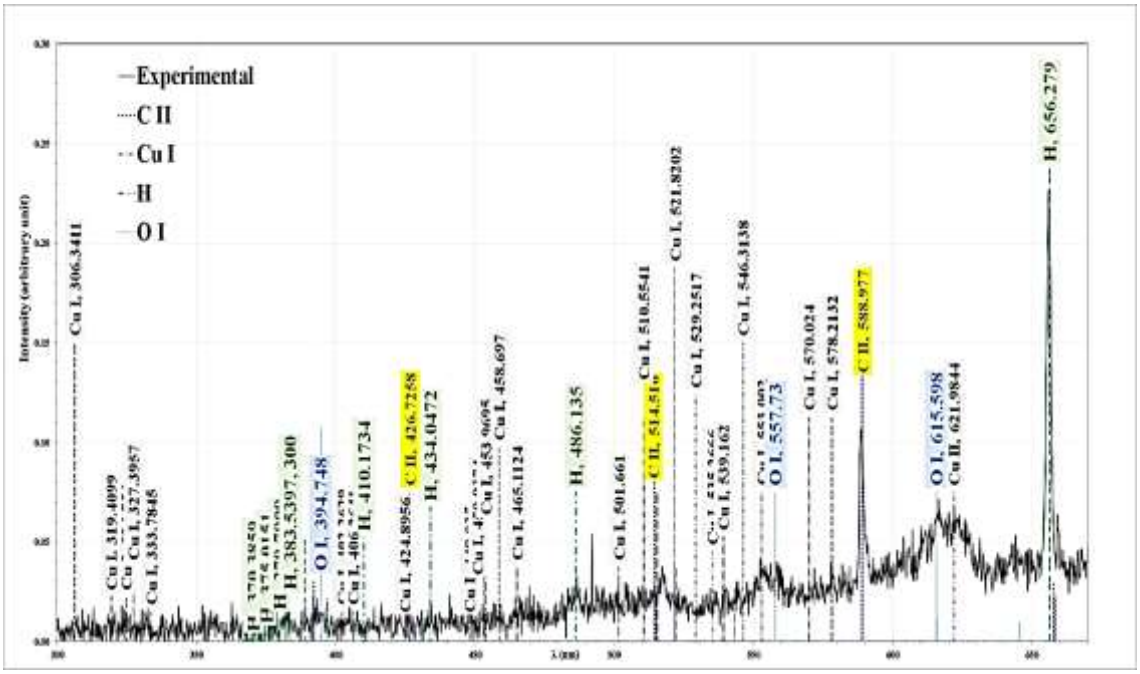

Figure 8: Emission spectrum for carbon exploding in CuO NP aqueous suspension.

Fig.8 shows the peak profile of the Hα line emitted from exploding graphite electrodes in CuO suspension. The line broadening (Δλ) was measured by Lorentzian fitting. Δλ was utilized to measure the electron density using the electron impact parameter for this line from previous studies [18].

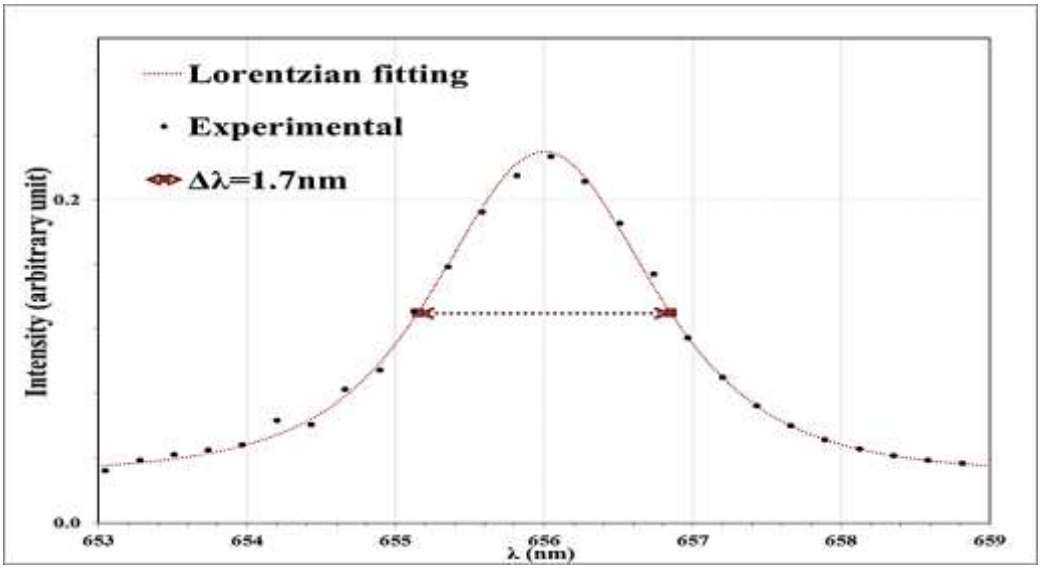

Figure 8: Lorentzian fitting for H_α line.

Electron temperature (T_e) was calculated by means of Boltzmann plot using the atomic spectral lines of argon, from the slope of best linear fitting of the relation between $Ln\left(\frac{I_{ji}\lambda_{ji}}{hcg_jA_{ji}}\right)$ versus the upper energy levels as shown in Fig.9 and using the details of lines data shown in Table 2 from National Institute of Standard and Technology Site (NIST) data for the wavelength, probability of transition multiply the statistical weight of excitation levels (g_kA_{ki}), lower level energy (E_i), and upper level energy (E_j) [19].

Table 2: Line parameters from NIST website.

Wavelength	g_kA_{ki}	E_i *(eV)*	E_j *(eV)*
306.3411	6.20×10^6	1.6422256	5.6883110
465.1124	3.04×10^8	5.0720890	7.7370270
510.5541	8.00×10^6	1.3889476	3.8166920
515.3235	2.40×10^8	3.7858976	6.1911751
521.8202	4.50×10^8	3.8166920	6.1920251
529.2517	8.72×10^7	5.3950500	7.7370270
570.024	9.60×10^5	1.6422256	3.8166920
578.2132	3.30×10^6	1.6422256	3.7858976

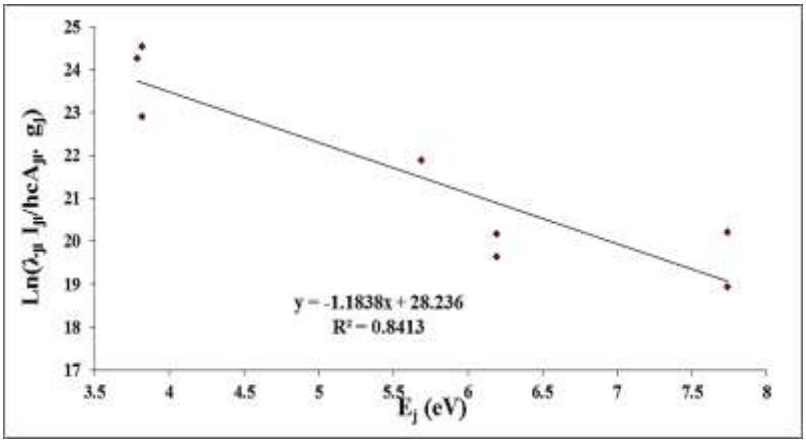

Figure 9: Boltzmann plot for Cu(I) lines produced by exploding graphite.

Table 3 shows the calculated values of electron temperature T_e, plasma density N_e, Debye length λ_D, plasma frequency f_p and Debye number N_D for emission from exploding graphite in the copper oxide suspensions.

Table 3: Plasma parameters for exploding graphite electrodes in oxide copper suspensions.

T_e (eV)	FWHM (nm)	$N_e \times 10^{16}$ (cm^{-3})	f_p (Hz) $*10^{12}$	λ_D $*10^{-6}$(cm)	N_d
0.845	1.700	8.50	2.618	2.342	5

4. Conclusions

In this work, a process of preparing composite of copper oxide particles with carbon was carried out in a simple and economical way, which is the process of exploding graphite electrodes in an aqueous suspension of copper oxide. The study showed a significant change in the particle properties after the composite preparation. The optical results showed that C-saturated CuO particles respond more strongly to visible light than the pure particles, and thus prefer visible light absorption, as the absorption spectrum showed a significant increase after the exploding process. In addition, the direct band gap decreased from 2.55 to 2.4 eV, while the indirect bandgap decreased from 1.1 to 1 eV, for CuO particles, after preparing C-CuO nanoparticles.

Acknowledgements

The authors are grateful to Department of Physics, College of Science, University of Baghdad and Ministry of Science and Technology.

Conflict of interest

The authors have no conflict of interest to declare.

References

1. Fikry M., Tawfik W., and Omar M.M., *Investigation on the effects of laser parameters on the plasma profile of copper using picosecond laser induced plasma spectroscopy.* Optical Quantum Electronics, 2020. **52**(5): pp. 1-16.
2. Tu B., Li M., Lu Q., Yang Y ,.Yao K., Lu D., Shen Y., Chen C., Hutton R., and Zou Y., *Simulating a low-temperature Maxwellian plasma using SH-HtscEBIT.* Physics Letters A, 2018. **382**(37): pp. 2673-2676.
3. Hamed S., *Spectroscopic determination of excitation temperature and electron density in premixed laminar flame.* Egypt. J. Solids, 2005. **28**(2): pp. 349-357.

4. Stambulchik E., Kroupp E., Maron Y., and Malka V., *On the Stark Effect of the OI 777-nm Triplet in Plasma and Laser Fields.* J Atoms, 2020. **8**(84): pp. 1-9.
5. Ni S., Chen Y., Li C., Zhang Z., Ning H., Kong X., Wang B., and Hosseinpour M., *Plasma emission induced by electron cyclotron maser instability in solar plasmas with a large ratio of plasma frequency to gyrofrequency.* The Astrophysical Journal Letters, 2020. **891**(1): pp. 1-8.
6. Khabarov K., Nouraldeen M., Tichonov S., Lizunova A., Efimov A., and Ivanov V., *Modification of Aerosol Gold Nanoparticles by Nanosecond Pulsed-Periodic Laser Radiation.* Nanomaterials, 2021. **11**(10): pp. 1-19.
7. Wasfi A.S., Humud H.R., and Fadhil N.K., *Synthesis of core-shell Fe_3O_4-Au nanoparticles by electrical exploding wire technique combined with laser pulse shooting.* Optics Laser Technology, 2019. **111**: pp. 720-726.
8. Bien T., Gu W., Bac L., and Kim J., *Preparation and characterization of copper-graphite composites by electrical explosion of wire in liquid.* Journal of Nanoscience Nanotechnology, 2014. **14**(11): pp. 8750-8755.
9. Kang J., Kim Y., Kim H.-m., Hu X., Saito N., Choi J.-H., and Lee M.-H., *In-situ one-step synthesis of carbon-encapsulated naked magnetic metal nanoparticles conducted without additional reductants and agents.* Scientific reports, 2016. **6**(1): pp. 1-9.
10. Gao X., Xu C., Yin H., Wang X., Song Q., and Chen P., *Preparation of graphene by electrical explosion of graphite sticks* .Nanoscale, 2017. **9**(30): pp. 10639-10646.
11. Bragg W.H. and Bragg W.L., *X rays and crystal structure*. 1918: G. Bell.
12. Scherrer P., *Göttinger Nachrichten.* Universität zu Göttingen, 1918. **2**: pp. 98-102.
13. Wang F., Liang L., Shi L., Liu M., and Sun J ,.*CO_2-assisted synthesis of mesoporous carbon/C-doped ZnO composites for enhanced photocatalytic performance under visible light.* Dalton Transactions, 2014. **43**(43): pp. 16441-16449.
14. Ding X., Zeng D., Zhang S., and Xie C., *C-doped WO_3 microtubes assembled by nanoparticles with ultrahigh sensitivity to toluene at low operating temperature.* Sensors Actuators B: Chemical, 2011. **155**(1): pp. 86-92.
15. Chen M.X., Zhu M., Zuo M., Chu S.Q., Zhang J., Wu Y., Liang H.W., and Feng X., *Identification of catalytic sites for oxygen reduction in metal/nitrogen-doped carbons with encapsulated metal nanoparticles.* Angewandte Chemie, 2020. **132**(4): pp. 1644-1650.
16. Sahai A., Goswami N., Kaushik S., and Tripathi S., *Cu/Cu_2O/CuO nanoparticles: Novel synthesis by exploding wire technique and extensive characterization.* Applied Surface Science, 2016. **390**: pp. 974-983.
17. Shibkov V., Shibkova L., and Logunov A., *The electron temperature in the plasma of a dc discharge created in a supersonic airflow.* Moscow University Physics Bulletin, 2017. **72**(3): pp. 294-300.
18. Mijatović Z., Djurović S., Gavanski L., Gajo T., Favre A., Morel V., and Bultel A., *Plasma density determination by using hydrogen Balmer Hα spectral line with improved accuracy.* Spectrochimica Acta Part B: Atomic Spectroscopy, 2020. **166**: pp. 1-8.
19. *NIST Atomic Spectra Database*. http://kinetics.nist.gov/index.php.

مزيج جسيمات أكسيد النحاس النانوية مع الكربون عن طريق تفجير قضيب جرافيت في معلقات مائية

سوسن حسين عبدالله[1]، حمد رحيم حمود[2], فلاح ابراهيم مصطفى[3]
[2،1]قسم الفيزياء, كلية العلوم, جامعة بغداد, بغداد, العراق
[3]وزارة العلوم والتكنولوجيا, بغداد, العراق

الخلاصة

تم في هذا العمل دراسة تأثير تركيب جسيمات أكسيد النحاس مع الكربون على بعض خواصه البصرية. تم إجراء عملية التركيب عن طريق تفجير أقطاب الجرافيت في معلق مائي من أكسيد النحاس. تمت دراسة خصائص البلازما المتكونة أثناء الانفجار باستخدام التحليل الطيفي للانبعاثات من أجل تحديد أهم العناصر الموجودة في الوسائط. تم تحديد كثافة الإلكترونات وطاقتها، والتي تعد العامل الرئيسي في عملية التركيب. تمت دراسة خصائص الجسيمات قبل وبعد عملية التفجير. أظهرت قياسات حيود الاشعة السينية ذروة إضافية في نمط أكاسيد النحاس المقابلة لهيكل الجرافيت السداسي للمركب. أظهر طيف الامتصاص للأشعة المرئية- فوق البنفسجية تحسنًا ملحوظًا بعد عملية التركيب. انخفضت فجوة النطاق المباشرة من 2.55 إلى 2.4 الكترون-فولت، وانخفضت فجوة النطاق غير المباشرة من 1.1 إلى 1 الكترون-فولت للمركب.